ISSN 0016-7029, Geochemistry International, 2007, Vol. 45, No. 10, pp. 971–982. © Pleiades Publishing, Ltd., 2007.
Original Russian Text © Yu.A. Kostitsyn, V.N. Volkov, D Z. Zhuravlev, 2007, published in Geokhimiya, 2007, No. 10, pp. 1057–1069.

Trace Elements and Evolution of Granite Melt as Exemplified by the Raumid Pluton, Southern Pamirs

Yu. A. Kostitsyn[a], V. N. Volkov[b], and D. Z. Zhuravlev[c]

[a] *Vernadsky Institute of Geochemistry and Analytical Chemistry, Russian Academy of Sciences, ul. Kosygina 19, Moscow, 119991 Russia*

e-mail: kostitsyn@geokhi.ru

[b] *Institute of Geology of Ore Deposits, Petrography, Mineralogy, and Geochemistry, Russian Academy of Sciences, Staromonetnyi per. 35, Moscow, 119017 Russia*

[c] *Institute of Mineralogy, Geochemistry, and Crystal Chemistry of Rare Elements, ul. Veresaeva 15, Moscow, 121357 Russia*

Received May 30, 2006

Abstract—New trace element data were obtained by ICP-MS for 58 samples representing eight intrusive phases of the Raumid granite Pluton. All of the rocks, except for one sample that was deliberately taken from a greisenized zone, were not affected by postmagmatic fluid alteration. The sequential accumulation of incompatible trace elements (Rb, Ta, Nb, Pb, U, and others) in the Raumid Pluton from the early to late phases coupled with a decrease in incompatible element contents (Sr, Eu, Ba, and others) indicates a genetic link between the granites of all phases via fractional crystallization of a granite melt. The REE distribution patterns of final granite phases are typical of rare-metal granites. The Ta content in the granites of phase 8 is only slightly lower than that of typical rare-metal granites. Greisenization disturbed the systematic variations in trace element distribution formed during the magmatic stage. The ranges of trace element contents (Rb, Sr, Ta, Nb, and others) and ratios (Rb/Sr, La/Lu, Eu/Eu*, and others) in the Raumid granite overlap almost entirely the ranges of granitic rocks of various compositions, from the least differentiated with ordinary trace element contents to rare-metal granites. This indicates that the geochemical signature of rare-metal granites can develop at the magmatic stage owing to fractional crystallization of melts, which is the case for the melt of the Raumid granite.

DOI: 10.1134/S0016702907100023

INTRODUCTION

According to modern geological concepts, there are only a few types of natural processes that can produce granites with high contents of trace elements. Many fundamental studies have demonstrated an important role of postmagmatic metasomatic alterations of granites for the formation of rare-metal ores [e.g., 1–3]. There is also a concept that the composition of the Earth's crust, including trace element contents, is affected by deep-seated fluids [4, 5]. However, there is convincing evidence that trace elements may be extensively accumulated in the course of granite melt evolution without any influence of a fluid phase (or before its appearance) [6, 7].

Many rare-metal granites bear evidence of postmagmatic alteration, which also affected trace element distribution. This is, perhaps, the main reason for the longstanding controversy between the magmatic and metasomatic concepts of their formation. It is obvious that the role of magmatic processes and, in particular, fractional crystallization in the accumulation of trace elements can be evaluated by studying an object in which postmagmatic fluid alterations are absent or occur only locally but the evolution of a single magmatic chamber can be reliably tracked. These requirements are met in the Raumid Pluton. According to the field observations that have been gained for many years, the Pluton was formed by eight phases of emplacement of cogenetic melts [8, 9], and its granites are practically free of postmagmatic alterations (microclinization, albitization, greisenization, etc.), which could have caused the trace element enrichment. A rapid mechanical erosion under conditions of a high mountain relief provided access to completely unweathered rocks.

In this paper, we report the concentrations of trace elements in 58 granite samples representing all of the eight intrusive phases of Raumid Pluton formation and consider possible reasons for the evolution of trace-element characteristics of these rocks.

BRIEF CHARACTERISTICS OF THE PLUTON AND ITS GRANITES

The Raumid Pluton of biotite leucogranites is located on the northern slope of the Rushan Range, within the Rushan–Pshart structural zone of the southern Pamirs. In the regional magmatic schemes, it was assigned to the Raumid intrusive complex, which was isotopically dated at the end of the Eocene [8]. The Pluton is an oval-shaped body, 100 km^2 in area. It is cut by

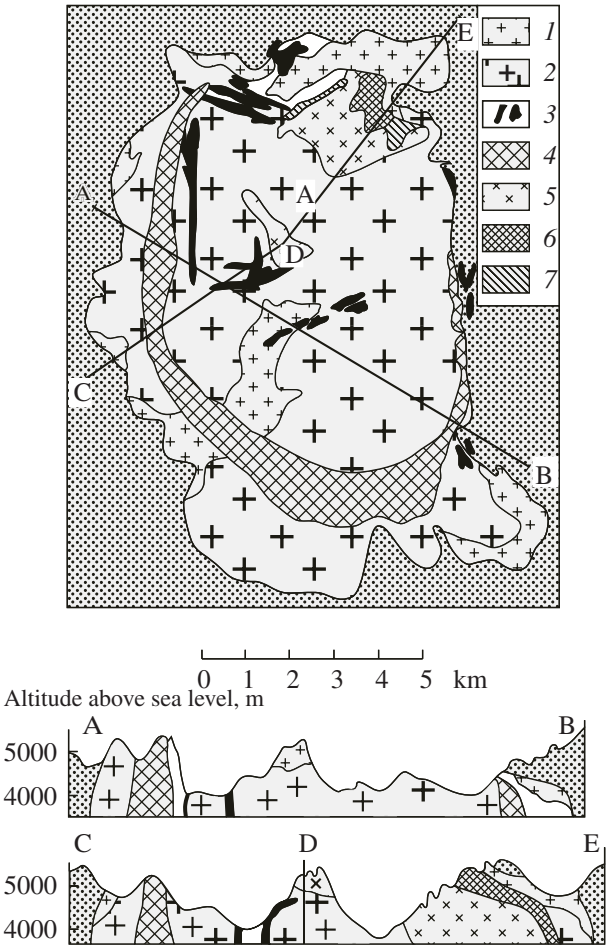

Fig. 1. Geological sketch map of the Raumid Pluton after Volkov [9]. Numbers denote intrusive phases. The granites of intrusive phase 8 occur as small bodies, which cannot be shown at the map scale.

river valleys to a depth of about 2 km, which revealed its domal shape with steep walls and a gently dipping roof preserved at the periphery of the Pluton. The Pluton has sharp contacts with the country metamorphosed sedimentary sequences and discordantly cuts folds in them. The country rocks are hornfelsed and locally greisenized, whereas granitization was not observed.

The Pluton has a complex structure related to its multistage emplacement. The granites of all of the eight phases are similar in appearance but have intrusive relations with each other. The order of phase formation was determined from the presence of xenoliths, apophyses, and veins of one phase in the intrusions of others. The shape, size, and allocation of different phases are shown in Fig. 1. The Pluton and its contact zone contain veins of amazonite pegmatites and quartz and greisen veins with fluorite, molybdenite, and beryl.

The Rb–Sr isotopic ages of granites of phases 2, 4, and 5 are 40.0 ± 2.7, 39.4 ± 2.0, and 35.1 ± 1.1 Ma, respectively [10]; however, the reported confidence intervals could be distorted owing to the incomplete homogenization of Sr isotopic composition during granite formation.

The constituent rocks are two-feldspar subalkaline leucogranites with a massive structure and a porphyritic texture (except for the aphyric fine-grained granites of phase 8). The phenocrysts are oligoclase, microcline perthite, quartz, and biotite. The groundmass is built up of the same minerals, but the groundmass plagioclase is more sodic and microcline has higher K, Rb, and Cs but lower Ba and Sr contents. This fact and the absence of phenocrysts in the granites of contact zones indicate the magmatic origin of phenocrysts and their crystallization during an early stage of magma solidification [9]. Allanite, zircon, apatite, thorite, fluorite, fergusonite, and monazite are the most common accessory minerals. All the granites contain small amounts (2–5 %) of minerals formed at a late magmatic stage or during high-temperature autometamorphism. These are perthitic albite and albite–quartz myrmekitic reaction rims between plagioclase and microcline, as well as muscovite and accessory fluorite. Muscovite occurs in negligible amounts and becomes significant only in the phase 6 granites. The magmatic minerals of the rocks are well preserved, and only slight pelitization of microcline, local saussuritization of plagioclase, and chloritization of biotite were observed.

The study of phases 2 and 5 revealed a vertical zoning in the distribution of many trace elements and some minerals [9, 11, 12]. From top to bottom, the contents of Ba, Sr, Ti, allanite, zircon, apatite, and early major rock-forming minerals (porphyritic phenocrysts) increase, whereas the contents of rare metals, F, monazite, and fluorite decrease. Such a zoning could result from either the gravitational settling of early crystals in the intrusive chamber or the filter pressing of magma during its emplacement. Variations in Rb and Sr contents in the granites of phase 5 with height are illustrated by Fig. 2.

SAMPLES, METHODS, AND ANALYTICAL RESULTS

Seven to ten representative 5–7-kg samples were taken from each intrusive phase for analysis. The samples of phase 5 span a more than 1-km-long vertical section. The analyzed samples were unaffected by any significant high-temperature postmagmatic alteration (see above). An exception is greisenized granite sample 971-2 from phase 8. The analysis of this sample was aimed at estimating the influence of postmagmatic fluid processes on trace element distribution.

Samples were hand crushed using an iron mortar and powdered in an agate mortar under alcohol.

The trace element compositions of 58 granite samples representing eight phases of the Pluton were determined by ICP-MS at the Institute of Mineralogy,

Geochemistry, and Crystal Chemistry of Rare Elements.

The samples were digested with acid in a MULTIWAVE microwave furnace. An aliquot of 50–100 mg was decomposed in a mixture of hydrofluoric and nitric acids in a Teflon vial at 260°C and a pressure of no more than 72 bar for 50 min. Metal fluorides were decomposed by digesting the dry residue mixed with 5–7 ml of 6.2 N HCl at 90°C for one hour. Subsequently, an internal standard (In) and 3 ml of 3 N HNO_3 were added to the sample. Chlorides were completely replaced by nitrates at 200°C within 15–20 min. The final concentration of HNO_3 was 0.5 N at a dilution factor of about 1000. This method provides the complete decomposition of the majority of magmatic, metamorphic, and sedimentary rocks, including acid-resistant minerals (zircon, monazite, and others).

Analytical grade and high-purity acids were preliminarily twice distilled in a quartz (Teflon for HF) apparatus.

The samples were analyzed using a Perkin Elmer Elan-6100 DRC mass spectrometer operated in a standard mode under the following conditions: 0.91–0.93 l/min nebulizer argon flow, 1.17 l/min auxiliary argon flow, 15 l/min plasma argon flow, 1270–1300 W operating plasma generator power, and 1000 V detector voltage in a counting mode.

The instrument was calibrated over the entire mass range using standard solutions containing all analyzed elements. In order to check the quality of measurements and take into account the drift of sensitivity, a standard was analyzed regularly after every 5–10 samples. A certified rock sample decomposed by the same method that was used for the rock samples served as an interlaboratory standard. The detection limits were 1–5 ng/g for the heavy- and medium-weight elements (U, Th, REE, etc.) and up to 20–50 ng/g for the light elements (Be, Sc, and others). The measurement error was 3–10% relative for the elements whose contents were 20–50 times the detection limit.

The obtained results are presented in the table. The contents of all elements are given in ppm. The Eu anomaly (Eu_n/Eu_n^*) was calculated using the following equation:

$$Eu_n^* = \sqrt{Sm_n \cdot Gd_n},$$

where the subscript *n* denotes values normalized to the chondrite [13].

The obtained data (table) indicate that the emplacement of the Raumid granites was accompanied by a significant evolution of their trace element composition. The general trend of this evolution is an increase in Ta, Nb, Be, U, Rb, Cs, Tl, Pb, Hf, Y, and HREE and a decrease in Ba, Sr, Zn, Th, Zr, LREE, and Eu. The contents of Ta, Nb, Be, U, Ba, and Sr in the granites of the late phases attain levels typical of Li–F granites [7], and the Ta content approaches the economic content of this element observed in Ta deposits in rare-metal granites.

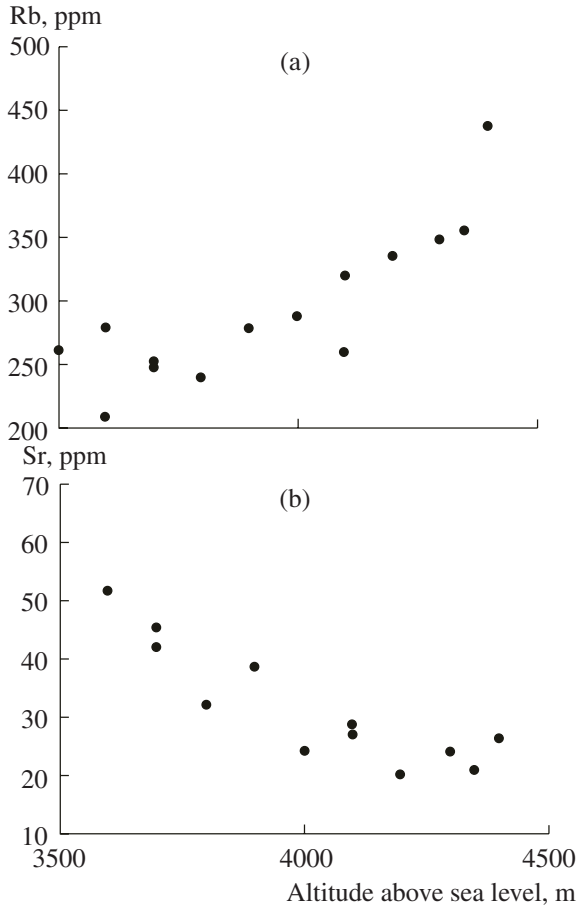

Fig. 2. Variations in the contents of (a) Rb and (b) Sr with sampling altitude in the granites of phase 5 of the Raumid Pluton (data from [10] are also shown).

DISCUSSION

There are mineralogical [11], petrographic [8], and geochemical [9, 12] indications that the evolution of the Raumid Pluton was controlled by fractional crystallization of an initial granite melt. Let us consider the behavior of trace elements during this process. If two elements, X and Y, have partition coefficients of D_X and D_Y, variations in their contents in a fractionating melt can be expressed trough their initial contents, $[X]_0$ and $[Y]_0$, and the degree of melt crystallization, *F*, as follows [14]:

$$\frac{[X]}{[X]_0} = F^{(D_X - 1)} \text{ and } \frac{[Y]}{[Y]_0} = F^{(D_Y - 1)},$$

which indicates that the rocks produced by the fractional crystallization of a single melt must display linear trends in the $\log(Y) - \log(X)$ diagram, and their slopes depend on the partition coefficients of the elements:

$$\frac{\log(Y)_1 - \log(Y)_2}{\log(X)_1 - \log(X)_2} = \frac{D_Y - 1}{D_X - 1}.$$

Trace element compositions of the granites of the Raumid Pluton

Element	117	309-1	842-1	846-1	848-1	902-4	903-1	907-3	P1	P22	25/74	868-1	872-1	921-1	933-1	949-1
Phase	1	1	1	1	1	1	1	1	2	2	2	2	2	2	2	2
Be	10.2	10.0	9.7	11.4	10.0	12.1	13.5	10.1	7.5	5.3	6.3	6.8	10.4	10.6	12.1	9.7
Sc	3.2	2.6	2.7	2.9	2.2	3.0	2.4	2.8	3.5	2.4	2.8	3.7	2.8	2.6	2.6	2.3
Cr	5.45	3.73	5.27	9.48	13.85	16.51	13.60	14.51	14.69	11.11	14.87	13.44	15.47	14.13	13.95	11.12
Co	1.45	1.00	1.50	2.02	1.33	2.27	1.56	2.09	1.72	1.41	1.36	1.30	1.22	1.08	1.30	1.66
Ni	3.12	2.38	2.97	5.30	12.93	15.10	12.62	13.23	13.33	11.52	8.45	7.25	8.35	8.41	7.89	5.42
Cu	10.48	3.97		3.78	4.65	8.23	3.81	6.50	2.79	3.76	3.76	5.12	4.02	10.32	8.36	
Zn	37.2	17.3	77.2	71.3	47.9	47.7	33.7	43.4	42.3	41.3	35.6	38.3	28.5	31.2	65.1	40.3
Ga	16.6	18.3	21.8	21.8	22.2	21.1	22.5	20.4	20.7	19.5	17.9	21.4	21.3	21.5	20.9	21.5
Rb	297	283	259	236	296	266	312	273	250	218	210	227	268	271	270	297
Sr	101	62	92	147	86	143	108	145	86	71	73	127	58	55	67	92
Y	26	32	36	27	40	39	37	19	34	18	26	27	31	47	48	52
Zr	82	149	127	54	111	134	107	122	125	69	113	66	47	101	93	147
Nb	43	32	46	38	55	55	54	44	55	39	34	38	43	59	56	73
Mo	0.66	0.75	0.63	0.64	1.64	1.00	1.43	0.67	0.70	0.87	0.49	0.64	0.40	1.05	0.39	0.34
Cs	4.1	3.1	3.2	3.2	4.7	4.0	4.9	4.1	3.8	2.4	3.1	3.4	3.7	3.3	8.4	5.5
Ba	248	177	212	463	221	285	253	300	180	132	132	310	110	112	218	191
Hf	2.78	5.21	5.39	2.40	4.05	4.51	4.28	3.97	4.07	2.30	3.85	2.12	2.03	4.26	3.78	5.11
Ta	8.36	6.88	6.38	5.57	8.01	6.90	8.61	5.61	5.14	2.50	3.05	3.09	5.13	7.68	6.61	7.43
W	0.92	9.77		2.33	4.69	1.75	1.76	1.03	1.03	0.60	0.76	1.06	0.85	1.23	1.07	1.52
Tl	1.38	1.14	1.12	1.07	1.35	1.04	1.39	1.12	1.05	0.91	0.87	0.99	1.08	1.23	1.31	1.37
Bi	1.34	0.14	0.13	0.07	0.21	0.21	0.30	0.85	0.10	0.03	0.42	0.05	0.22	0.44	0.25	0.10
Pb	26.0	34.5	35.8	36.2	30.8	24.4	32.5	27.6	31.1	26.5	26.1	30.6	32.7	35.6	37.6	39.5
Th	44.1	35.9	52.9	40.6	55.7	48.3	47.2	37.2	71.5	57.7	59.0	67.9	45.6	51.1	47.4	62.8
U	7.7	6.4	8.9	5.2	12.1	8.1	11.8	5.0	9.6	9.6	13.1	9.0	9.8	14.3	9.9	15.8
La	38.4	30.6	34.0	40.2	32.9	47.4	31.9	39.7	48.6	37.7	30.8	73.1	29.6	26.1	32.7	39.4
Ce	72.4	52.8	71.4	79.9	69.3	95.5	67.7	77.6	100.6	80.3	65.4	145.6	65.5	57.9	70.8	81.5
Pr	7.14	5.79	8.34	8.83	7.69	10.43	7.60	8.00	11.38	9.04	7.52	15.40	7.53	6.75	8.13	9.31
Nd	28.6	25.7	27.4	29.3	26.8	34.8	26.0	25.9	38.4	30.7	25.6	50.0	26.6	24.1	28.8	32.1
Sm	5.82	4.86	5.44	4.91	5.69	6.68	5.34	4.06	7.29	5.60	5.17	7.82	5.63	5.98	6.77	7.02
Eu	0.398	0.319	0.407	0.582	0.375	0.512	0.449	0.506	0.377	0.312	0.308	0.755	0.262	0.255	0.309	0.389
Gd	4.31	3.27	4.92	4.20	4.79	5.47	4.39	2.97	5.82	4.05	4.06	5.68	4.55	5.49	5.99	6.55
Tb	0.766	0.643	0.784	0.617	0.837	0.911	0.754	0.444	0.902	0.571	0.643	0.807	0.741	1.013	1.074	1.156
Dy	3.86	4.93	5.33	4.21	5.09	5.36	4.62	2.47	5.17	2.91	3.68	4.32	4.28	6.52	6.69	7.27
Ho	0.96	1.08	1.02	0.78	1.12	1.13	1.05	0.53	1.07	0.57	0.76	0.85	0.89	1.44	1.46	1.63
Er	2.66	2.34	2.96	2.28	3.25	3.29	3.12	1.63	2.87	1.52	2.08	2.35	2.46	3.98	4.02	4.58
Tm	0.337	0.435	0.537	0.377	0.525	0.522	0.526	0.273	0.433	0.214	0.323	0.352	0.390	0.651	0.641	0.734
Yb	3.15	3.41	3.16	2.22	3.52	3.46	3.60	1.91	2.73	1.38	2.08	2.25	2.51	4.19	4.24	4.66
Lu	0.421	0.378	0.485	0.337	0.509	0.512	0.564	0.304	0.383	0.206	0.308	0.333	0.363	0.608	0.604	0.669
$(La/Lu)_n$	9.46	8.40	7.28	12.38	6.70	9.61	5.88	13.54	13.16	18.98	10.39	22.81	8.48	4.46	5.63	6.12
Eu_n/Eu^*_n	0.24	0.24	0.24	0.39	0.22	0.26	0.28	0.44	0.18	0.20	0.20	0.35	0.16	0.14	0.15	0.18

Table. (Contd.)

Element	118-2a	814-2	814-3	817-1	822-2	824-1	961-1	961-3	893-1	100	106-1	106-4	119	120	867-1	956-1
Phase	3	3	3	3	3	3	3	3	3	4	4	4	4	4	4	4
Be	7.8	11.7	10.4	7.8	6.7	7.2	9.1	6.8	10.5	6.7	7.5	6.4	7.6	6.1	8.2	7.1
Sc	1.8	2.0	3.0	2.3	1.9	2.3	3.0	2.3	2.4	2.5	2.0	1.9	1.4	2.0	1.9	1.6
Cr	10.74	12.00	23.89	9.63	11.68	25.16	18.99	26.33	25.18	2.68	2.18	2.14	1.27	1.52	2.89	1.15
Co	1.35	1.11	1.67	1.06	0.91	0.91	1.64	1.35	1.09	1.31	0.99	1.10	0.50	1.01	0.84	0.51
Ni	5.21	5.96	5.81	4.44	5.47	15.24	10.93	15.06	14.05	1.57	1.23	1.39	1.11	1.11	1.16	1.42
Cu	9.86		2.91	2.05	3.16	3.21	2.92	4.96	4.79	5.16	4.75	3.96	4.67	8.08	4.87	
Zn	41.0	152.2	34.7	21.1	22.9	27.9	38.0	36.4	31.0	50.2	41.5	51.0	29.4	27.3	26.5	2207.3
Ga	20.2	20.1	22.2	19.9	20.2	19.0	21.8	19.3	21.0	20.6	17.7	18.1	18.2	19.9	23.5	23.0
Rb	202	252	229	191	243	236	254	249	271	229	263	239	241	215	228	269
Sr	74	31	95	56	23	45	84	73	60	127	96	105	44	82	54	36
Y	41	65	47	46	46	33	28	24	49	30	18	20	30	14	32	40
Zr	104	82	111	86	89	80	140	28	107	114	92	104	111	104	114	96
Nb	59	53	57	59	68	45	42	35	60	36	28	29	32	23	42	42
Mo	0.33	1.39	0.42	0.21	0.31	0.59	0.56	0.61	0.60	0.16	0.09	0.12	0.08	0.87	0.33	0.27
Cs	1.7	2.5	2.8	2.5	2.1	2.7	4.7	2.7	3.1	3.5	6.7	3.5	3.2	4.5	3.0	4.0
Ba	145	56	154	75	42	73	163	133	112	292	176	216	93	130	97	71
Hf	4.23	3.13	4.28	3.63	3.54	3.08	4.88	1.21	4.24	4.38	3.10	3.45	4.31	3.81	4.81	4.54
Ta	7.00	10.53	7.72	7.47	5.23	4.83	4.28	4.03	6.51	4.35	3.27	2.31	4.05	1.41	3.71	5.72
W	0.78		1.95	1.26	1.56	2.37	0.43	0.99	1.10	1.33			1.00		0.37	3.58
Tl	0.81	1.00	0.86	0.74	0.90	0.91	1.13	1.01	1.14	1.01	1.52	1.34	1.20	1.16	1.05	1.19
Bi	0.07	0.04	0.07	0.07	0.17	0.46	0.12	0.06	3.85	0.09	0.11	0.09	0.08	0.07	0.06	0.09
Pb	25.6	37.1	25.9	25.5	26.0	29.1	31.8	31.5	35.2	47.9	43.6	38.2	40.5	32.2	42.8	51.4
Th	48.8	51.9	49.1	41.6	38.4	45.7	58.4	46.8	46.1	65.5	84.5	72.0	54.0	80.0	79.3	55.5
U	12.4	17.8	14.2	12.1	13.8	9.4	10.1	8.9	12.6	14.7	14.2	13.3	10.9	15.0	14.5	13.0
La	32.0	18.9	36.3	26.5	15.6	27.8	41.3	29.4	29.4	61.3	61.6	46.4	27.9	39.3	39.5	29.0
Ce	68.1	45.4	75.5	59.0	37.9	59.3	85.5	62.5	64.4	115.0	129.6	100.8	61.4	91.8	91.6	66.9
Pr	7.59	5.75	8.55	7.07	4.69	6.60	9.48	6.88	7.61	14.87	14.04	11.47	7.20	10.90	11.94	8.82
Nd	26.3	23.1	29.7	26.0	18.3	22.9	31.7	24.1	27.2	49.3	44.2	32.0	26.5	28.4	36.6	29.2
Sm	5.68	7.16	6.59	6.42	5.40	4.88	5.87	4.72	6.51	7.11	7.35	6.04	5.78	5.16	6.17	5.90
Eu	0.328	0.175	0.374	0.246	0.113	0.197	0.348	0.317	0.265	0.685	0.465	0.549	0.242	0.499	0.392	0.256
Gd	5.20	7.13	5.80	5.69	5.58	4.23	4.48	3.61	5.95	5.91	5.88	5.19	4.63	4.35	5.97	5.39
Tb	0.922	1.335	1.002	1.011	1.066	0.730	0.697	0.571	1.076	0.799	0.740	0.694	0.832	0.514	0.753	0.778
Dy	5.94	8.89	6.05	6.31	7.01	4.50	3.93	3.43	6.93	5.41	3.10	3.31	4.82	2.24	5.37	5.46
Ho	1.30	1.96	1.37	1.37	1.57	0.97	0.82	0.71	1.53	1.03	0.66	0.65	1.01	0.44	0.89	1.06
Er	3.71	5.35	3.76	3.81	4.20	2.71	2.31	1.95	4.18	2.53	2.00	2.05	2.79	1.49	2.56	2.93
Tm	0.595	0.866	0.593	0.598	0.636	0.420	0.362	0.312	0.652	0.471	0.240	0.266	0.422	0.216	0.491	0.563
Yb	3.78	5.74	3.90	3.97	3.83	2.68	2.49	2.10	4.27	2.67	1.95	1.97	2.98	1.29	2.34	3.10
Lu	0.544	0.809	0.556	0.564	0.540	0.399	0.365	0.302	0.604	0.376	0.317	0.339	0.433	0.235	0.386	0.478
$(La/Lu)_n$	6.11	2.42	6.79	4.87	3.00	7.22	11.75	10.08	5.05	16.95	20.20	14.19	6.68	17.40	10.61	6.31
Eu_n/Eu_n^*	0.18	0.07	0.18	0.12	0.06	0.13	0.21	0.23	0.13	0.32	0.22	0.30	0.14	0.32	0.20	0.14

Table. (Contd.)

Element	939-2	858-1	859-1	834-1	111	110	112	863-1	828-2	828-5	903-A	903-B
Phase	5	5	5	5	5	5	6	6	6	6	6	6
Be	9.5	8.6	8.1	9.0	9.8	11.0	11.0	14.2	12.2	11.6	16.3	15.8
Sc	2.6	2.0	6.6	2.6	2.7	3.1	2.7	2.9	2.8	2.6	2.8	2.7
Cr	2.00	2.96	5.92	2.02	2.48	3.49	2.65	5.33	8.02	2.10	1.09	2.54
Co	0.83	0.52	0.77	0.42	0.50	0.58	0.50	0.42	0.70	0.51	0.45	0.35
Ni	2.98	1.40	8.04	1.38	1.32	1.27	2.46	3.69	5.96	2.24	1.12	0.95
Cu	14.16	14.74			10.95	5.24	3.00	6.45	5.04	4.51	5.69	13.96
Zn	27.8	27.0	256.0	59.6	29.1	26.0	19.4	22.3	22.6	16.8	52.2	17.3
Ga	22.5	17.8	24.7	18.9	20.3	24.1	26.1	27.4	27.9	27.7	25.0	22.4
Rb	248	240	288	335	355	319	398	416	407	419	353	380
Sr	42	32	24	20	21	27	16	14	13	16	6.0	10
Y	39	36	53	57	66	57	73	105	94	85	104	75
Zr	70	67	87	89	89	95	103	103	133	85	111	118
Nb	51	49	58	78	96	85	88	93	87	106	81	84
Mo	1.48	0.52	1.66	1.44	0.08	0.08	0.27	0.19	0.29	0.12	0.29	0.05
Cs	3.5	2.2	4.3	4.7	5.6	4.3	6.9	6.2	5.5	10.8	4.3	5.6
Ba	72	54	42	63	61	68	37	36	40	34	27	27
Hf	3.80	2.50	5.23	3.91	4.65	5.51	7.47	8.15	9.07	6.12	8.50	7.41
Ta	4.86	6.54	9.61	11.58	14.30	8.31	13.38	15.75	16.86	17.75	21.20	23.61
W	0.80				6.87	2.65	3.53	4.14	5.63	8.76	5.28	
Tl	1.21	1.18	1.13	1.66	1.87	1.56	2.04	2.10	1.70	1.99	1.38	1.81
Bi	0.43	0.46	0.53	0.55	0.13	0.17	0.60	0.39	0.23	2.03	0.48	4.45
Pb	33.4	39.9	48.8	53.0	42.7	39.8	50.9	55.5	65.1	41.9	58.9	45.1
Th	63.2	44.3	32.9	38.0	40.0	43.0	37.9	36.2	33.0	36.2	29.4	33.2
U	17.2	10.3	14.8	17.1	21.6	20.3	20.4	23.3	29.8	26.4	19.3	21.6
La	32.9	22.0	13.5	12.6	14.3	15.5	9.6	9.4	9.3	9.9	8.4	8.0
Ce	80.0	49.2	33.6	32.4	37.8	43.5	27.4	28.6	26.9	30.1	23.1	22.7
Pr	10.61	5.36	5.39	4.09	4.93	5.90	4.02	4.44	4.45	4.76	4.09	3.09
Nd	32.6	24.6	19.7	17.3	20.0	18.5	14.7	17.3	17.9	16.6	19.7	14.9
Sm	7.76	6.05	5.45	6.43	7.62	5.81	6.10	6.96	5.92	7.70	8.21	6.85
Eu	0.231	0.147	0.147	0.096	0.106	0.167	0.094	0.091	0.098	0.090	0.055	0.052
Gd	6.73	4.69	6.63	6.88	8.82	7.27	7.33	8.79	7.75	9.45	8.34	7.05
Tb	1.05	0.91	1.19	1.40	1.66	1.27	1.44	1.69	1.41	1.79	1.76	1.61
Dy	6.48	6.25	10.10	9.71	10.61	8.68	9.88	14.23	13.46	11.58	14.46	10.85
Ho	1.25	1.28	1.53	2.22	2.50	1.70	2.05	2.65	2.52	2.69	3.16	2.69
Er	4.06	3.32	4.43	6.07	6.94	5.37	6.48	7.98	8.70	8.14	8.75	7.35
Tm	0.621	0.486	0.932	0.879	0.987	0.93	1.15	1.66	1.55	1.47	1.60	1.15
Yb	3.39	3.66	3.82	6.37	7.01	4.84	6.49	8.35	7.57	8.03	9.50	9.10
Lu	0.498	0.472	0.592	0.844	1.00	0.77	1.03	1.41	1.15	1.28	1.18	1.31
$(La/Lu)_n$	6.85	4.84	2.37	1.56	1.48	2.10	0.97	0.69	0.84	0.80	0.74	0.63
Eu_n/Eu_n^*	0.10	0.08	0.07	0.04	0.04	0.08	0.04	0.04	0.04	0.03	0.02	0.02

Table. (Contd.)

Element	P4	825-1	838-2	860-1	311-3	821-2	821-3	826-2	837-1	854-1	861-2	864-1	893-2	972-1
Phase	7	7	7	7	8	8	8	8	8	8	8	8	8	8
Be	7.7	10.6	11.9	14.6	11.7	8.0	9.2	13.8	13.8	13.7	9.6	12.3	14.0	25.2
Sc	2.5	2.1	2.6	2.3	2.5	3.6	2.1	2.7	2.7	2.5	2.1	1.8	2.0	8.0
Cr	2.37	1.38	3.21	5.20	9.43	2.10	1.20	1.48	1.65	5.28	2.98	6.06	1.65	1.63
Co	0.75	0.58	0.44	0.44	0.38	0.35	0.24	0.38	0.35	0.31	0.25	0.19	0.34	0.12
Ni	2.27	1.72	1.24	2.95	4.20	2.14	0.92	1.68	1.30	3.31	1.48	3.26	1.77	1.09
Cu	5.22	6.99	2.08	12.31	4.47	5.51	3.08	3.37	10.43	1.94	14.43	5.58	4.15	3.13
Zn	17.0	25.6	17.0	36.2	7.7	13.1	16.3	45.0	19.9	80.5	14.7	19.4	17.0	18.8
Ga	20.4	21.2	22.0	25.0	19.4	17.8	17.3	23.8	25.7	23.6	18.8	19.1	21.9	28.7
Rb	269	282	309	389	273	223	239	353	331	369	383	397	342	464
Sr	38	19	12	18	12	13	13	9.1	5.1	10.0	5.9	5.8	8.7	2.4
Y	56	51	55	63	68	51	45	69	110	87	63	90	90	120
Zr	107	88	122	83	47	51	64	94	149	56	82	91	66	81
Nb	64	76	63	68	74	60	62	93	96	87	67	84	95	43
Mo	0.04	0.11	0.09	0.11	0.11	0.10	0.05	0.05	0.07	0.07	0.30	0.08	0.84	9.14
Cs	3.5	4.3	5.0	10.2	4.5	2.4	3.0	4.9	5.1	7.3	4.7	4.2	5.3	6.5
Ba	83	34	22	29	23	15	12		24		19	18	21	16
Hf	5.42	4.81	6.81	5.50	3.92	3.37	3.16	6.55	10.12	4.68	5.22	5.73	4.71	8.89
Ta	13.66	7.92	10.12	9.84	10.35	12.20	6.86	12.88	18.75	11.54	18.59	20.27	18.23	61.60
W	2.54	2.77	4.94	4.94	5.88	6.24	3.24	6.42		6.99	8.32	7.91	7.17	5.77
Tl	1.02	1.28	1.20	2.09	1.11	1.03	1.09	1.59	1.28	1.80	1.80	1.84	1.50	1.67
Bi	0.26	0.18	0.37	0.46	2.58	0.45	0.44	1.82	5.69	0.16	4.26	0.27	1.72	6.29
Pb	56.1	37.7	58.1	49.9	46.4	39.6	38.2	55.1	45.7	63.2	44.3	42.9	51.6	84.6
Th	33.6	45.4	33.8	36.9	23.6	18.7	31.1	24.0	37.9	27.4	27.5	27.5	23.3	17.6
U	20.4	17.6	18.8	21.7	21.2	13.4	18.3	24.0	33.1	27.5	15.1	17.6	27.1	19.2
La	20.8	13.8	15.7	10.8	4.6	3.3	7.0	8.5	6.8	10.0	4.9	5.3	2.4	10.1
Ce	42.3	37.5	35.6	31.3	13.6	11.5	21.8	22.9	21.7	28.5	13.6	17.1	9.3	29.9
Pr	5.76	5.42	5.10	4.77	2.25	1.82	3.25	3.38	3.63	4.16	1.81	2.47	1.79	5.02
Nd	22.4	18.4	20.3	17.2	12.2	11.7	14.3	14.2	17.6	16.8	10.9	14.7	9.5	24.8
Sm	5.32	6.51	5.77	5.78	5.82	6.59	6.69	5.86	8.29	7.47	5.77	8.42	6.79	9.49
Eu	0.207	0.110	0.083	0.111	0.072	0.071	0.075	0.067	0.041	0.079	0.036	0.026	0.046	0.015
Gd	5.51	7.13	5.29	7.26	5.58	6.70	6.84	7.02	9.50	8.73	5.36	8.90	8.21	7.74
Tb	1.06	1.30	1.11	1.23	1.39	1.49	1.34	1.41	1.89	1.75	1.40	2.09	1.84	1.79
Dy	9.45	7.80	9.01	7.87	10.38	8.79	7.34	10.95	15.06	11.97	9.30	12.52	11.43	15.19
Ho	1.82	1.76	1.92	1.78	2.51	2.27	1.98	2.37	3.21	2.64	2.51	3.48	2.98	3.27
Er	4.23	5.22	5.00	5.54	5.95	5.61	5.25	6.22	8.79	8.05	6.53	9.50	8.88	8.13
Tm	0.94	0.81	0.89	0.99	1.06	0.68	0.64	1.07	1.57	1.30	0.93	1.22	1.38	1.93
Yb	4.89	4.97	4.85	5.88	7.38	5.74	5.21	6.31	10.12	8.11	8.66	11.51	10.50	15.53
Lu	0.62	0.73	0.63	0.99	0.88	0.68	0.72	0.89	1.44	1.23	1.00	1.54	1.42	1.89
$(La/Lu)_n$	3.46	1.96	2.58	1.13	0.54	0.50	1.01	0.99	0.49	0.84	0.51	0.36	0.18	0.55
Eu_n/Eu_n^*	0.12	0.05	0.05	0.05	0.04	0.03	0.03	0.03	0.014	0.03	0.020	0.009	0.019	0.005

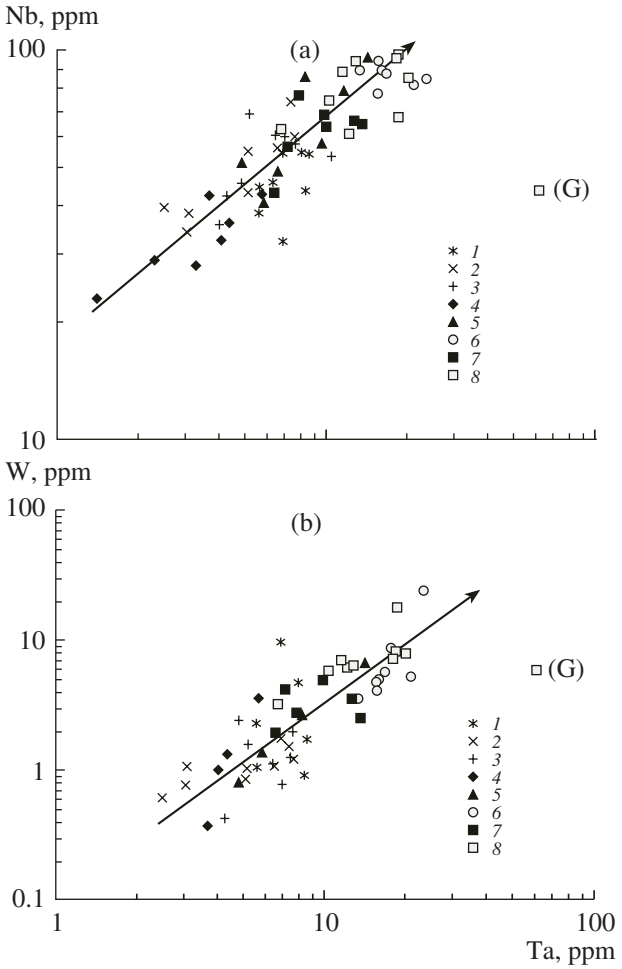

Fig. 3. Correlations between (a) Ta and Nb and (b) Ta and W in the granites of the Raumid Pluton. Numbers of intrusion phases are shown in the legend. Hereinafter, arrows show the direction of compositional evolution of the rocks from early to late stages. Only one point (G) corresponding to greisenized sample 972-1 of phase 8 significantly deviates from the general trend.

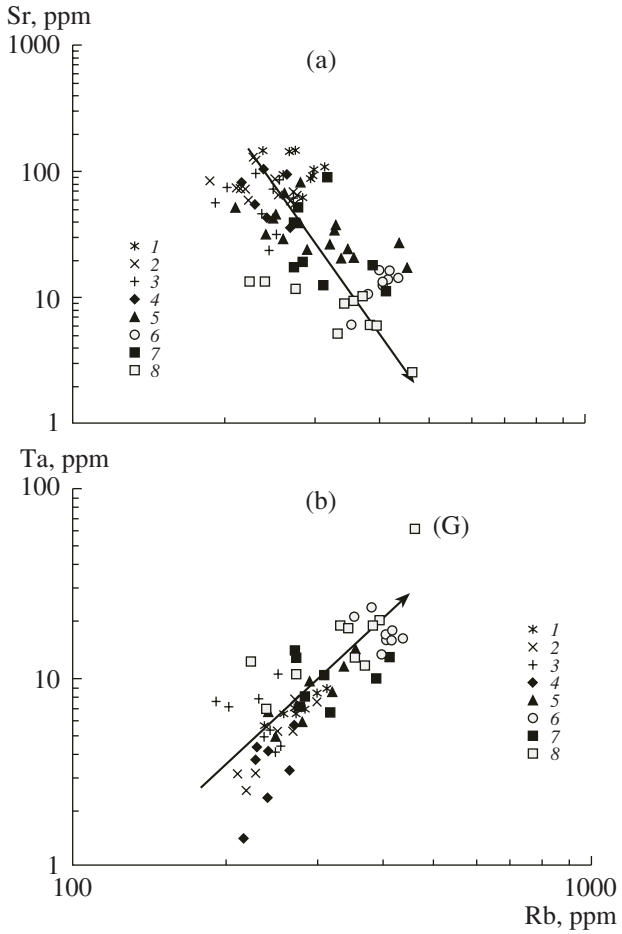

Fig. 4. Correlations between (a) Sr and Rb and (b) Ta and Rb in the granites of the Raumid Pluton.

Extended linear trends with an increase in incompatible elements and a decrease in compatible elements in trace element log(Y)–log(X) plots suggest that fractional crystallization is responsible for the observed variations in melt composition. The disturbance of these trends suggests a significant influence of other processes, such as contamination, magma mixing, and participation of the fluid phase during magmatic or postmagmatic stages.

As can be seen in the covariation diagrams (Figs. 3–5), the contents of Rb, Ta, W, and Nb increase from early to late phases in the Raumid Pluton, whereas Sr and Eu contents decrease. The distinct linear trends observed in the bilogarithmic plots are in agreement with the accumulation of incompatible elements (Rb, Ta, Nb, and W) and depletion in compatible elements (Sr and Eu) in the residual melt during fractional crystallization. Note that the composition of the greisenized granite of phase 8 plots far from the main trend of unaltered granites. Noteworthy is that the Ta content of the late granites approaches that of the rare-metal granite hosting Ta deposits.

The change in trace element contents in the subsequent intrusion phases is not monotonous but is complicated by compositional variability within each phase with considerable overlapping of ranges shown by particular phases. It is difficult to ascertain whether these variations were caused by different conditions of melting, magmatic evolution, or insufficiently representative sampling of different phases, which can be related to different degrees of exposure of the phases. However, the observed deviations from monotonic relations do not disturb the general variation trends of trace elements in the granites of various phases of the Raumid Pluton (Figs. 3–5), which are the focus of this study.

The trace element diagrams presented above provide convincing evidence that the observed trace element evolution of the granites of the Raumid Pluton was controlled by the fractional crystallization of a single melt, and this process was sufficiently efficient to accumulate rare metals in residual melts up to the levels typical of rare-metal granites. Except for one greisenized sample, the rocks bear no evidence for postmag-

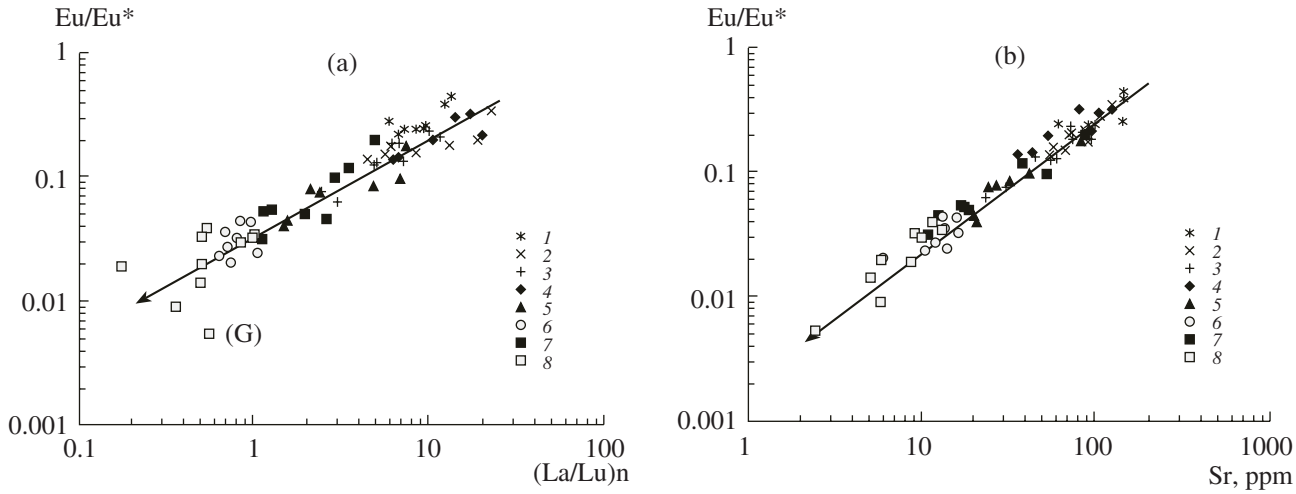

Fig. 5. Correlation between (a) the magnitude of Eu anomaly and La/Lu ratio and (b) Eu and Sr contents in the Raumid granites. The single trend of decreasing La/Lu and relative Eu content from early to late phases indicates a common evolution process.

matic processes and reflect trace element accumulation in the melts via fractional crystallization and melt movement relative to crystals during intrachamber intrusive activity.

As can be seen in Fig. 5a, the granites of various phases show a distinct correlation between La/Lu and the magnitude of Eu anomaly. This persistent trend suggests a common mechanism of melt evolution from early to late phases. The latest phases (from fourth to eighth) are characterized by the maximum compositional variations with a regular increase in the degree of differentiation. Only greisenized sample 972-1 (phase 8) again significantly deviates from the common trend.

The contents of Sr and Eu show a strong correlation (Fig. 5b) and decrease from early to late phases owing to the removal of these elements during the crystallization and partial elimination of feldspars.

The similarity of the ionic radii of divalent Eu and Sr [15] results in an almost identical partitioning of these elements into feldspar during the crystallization of silicate melt [16]. The slope of the trend shown in Fig. 5b is 0.9, i.e., only slightly different from 1. This implies that Sr was removed from the melt by crystallizing feldspars only a few percent more extensively than Eu. This difference could be related to a slight difference between the partition coefficients of Eu and Sr and to the fact that part of Eu occurs in the trivalent state and transforms to the divalent state as Eu^{2+} is removed from the melt.

The data obtained in this study are compared in Fig. 6 with Eu and Sr contents in various I- and S-type granites, including rare-metal granites and greisens [17]. It is clearly seen that they form a trend similar to that obtained for the Raumid granites (Fig. 5). The only dif-

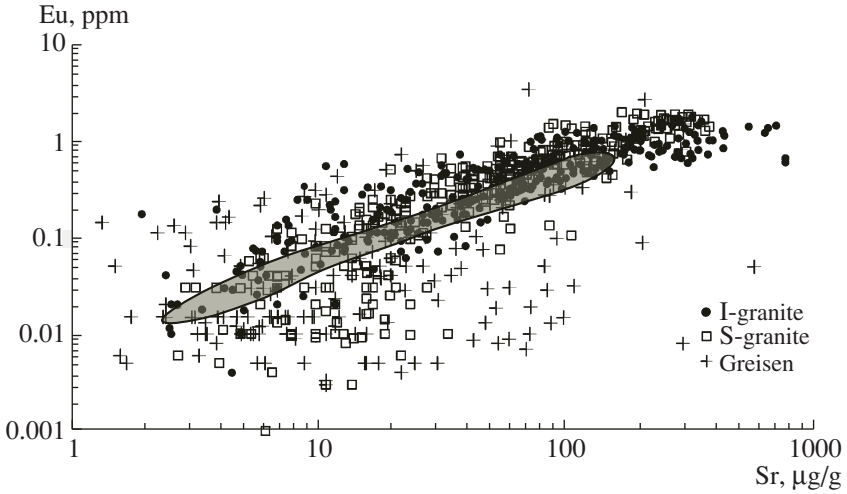

Fig. 6. Correlation between Eu and Sr contents in various granites of I- and S-types, including the most differentiated rare-metal granites and greisens. The sources of analytical data were reported in [17]. The outlined field represents the data for the Raumid granites.

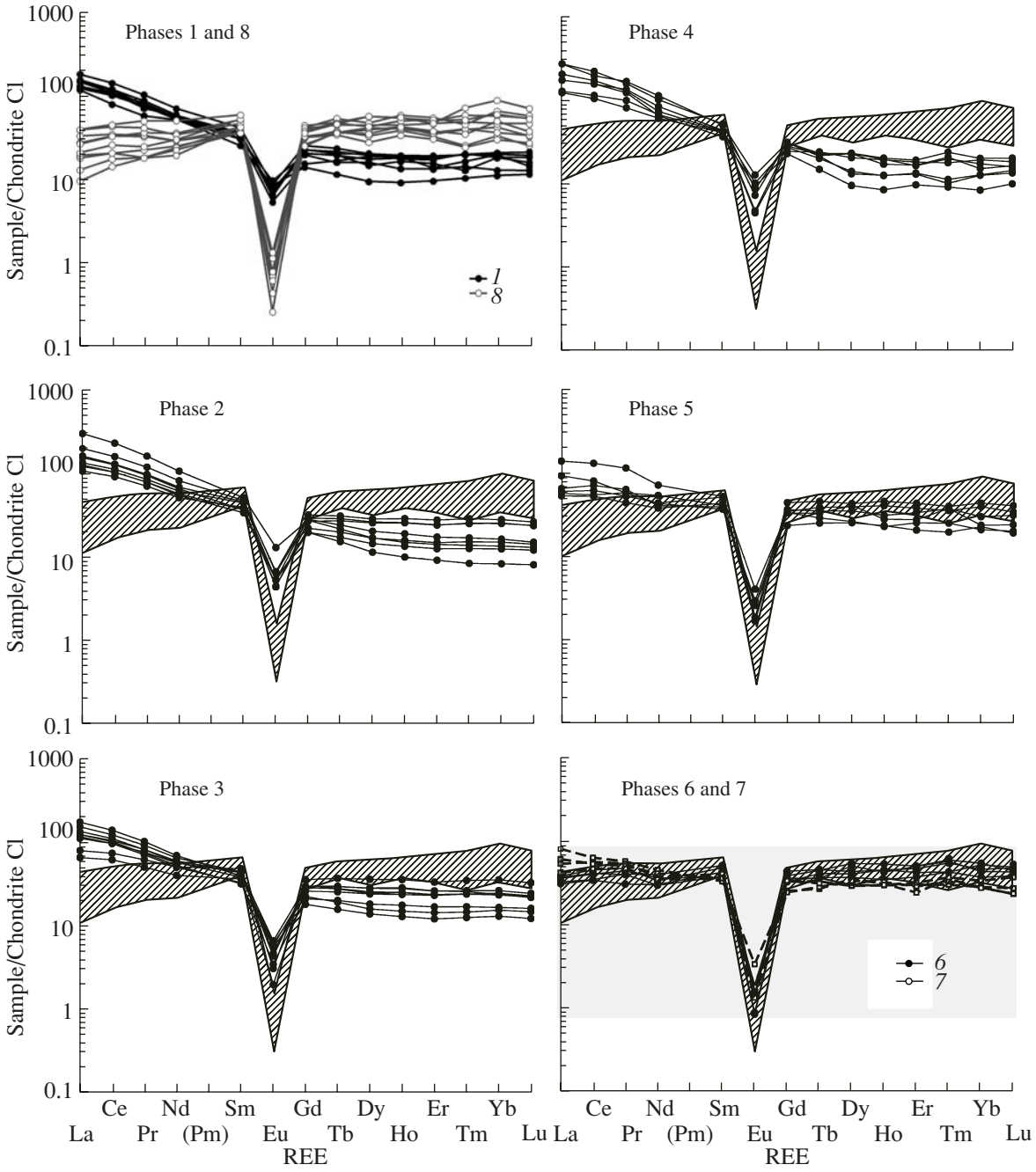

Fig. 7. Distribution patterns of REE in the granites of various phases of the Raumid Pluton as compared with the granites of phase 8.

ference that the trend in Fig. 6 is less consistent and disturbed primarily by the points of greisens and some rare-metal granites. Perhaps, the initial magmatic correlation between Sr and Eu that developed in each complex could be as strong as in the Raumid granites, and the deviation could be caused by variable postmagmatic greisenization typical of rare-metal granites. On the other hand, possible regional variations in trace element abundances in granitoids cannot also be ruled out.

Figure 7 shows the chondrite-normalized REE distribution patterns of various phases as compared with those of final phase 8. It is clearly seen that the REE composition of the granites gradually evolves from that typical of I-type granites with a moderate negative Eu anomaly ($Eu_n/Eu_n^* = 0.2–0.5$) and an LREE predominance over HREE [$(La/Lu)_n = 10–15$ in the granites of phase 1 (table)] to REE distribution patterns typical of highly evolved rare-metal granites [7, 17] with a strong

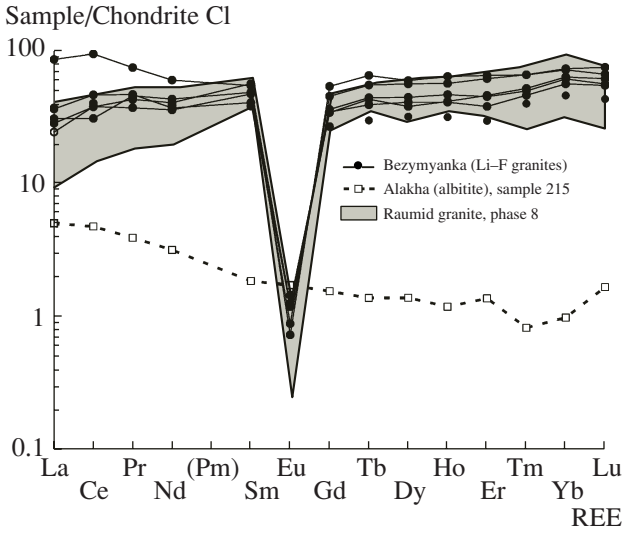

Fig. 8. Distribution patterns of REE in the Li–F granites of the Bezymyanka Pluton (western Transbaikalia) [7] and the albitite of the Alakha stock (southern Altai) [20]. The shaded field shows the granites of phase 8 of the Raumid Pluton.

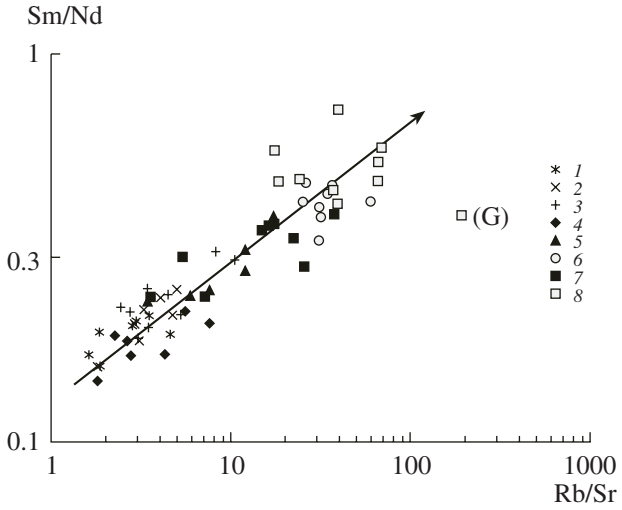

Fig. 9. Correlation between Sm/Nd and Rb/Sr ratios in the granites of various phases of the Raumid Pluton.

negative Eu anomaly (Eu_n/Eu_n^* = 0.01–0.04) and significant HREE enrichment, $(La/Lu)_n$ = 0.2–1.0. Such REE patterns in rare-metal complexes are explained by the extensive crystal fractionation of felsic magmas [7, 18, 19]. The data obtained for the granites of the Raumid Pluton strongly support this suggestion.

Figure 8 compares the chondrite-normalized REE patterns of the granites of phase 8 of the Raumid Pluton with those of the typical Li–F granites of the Bezymyanka complex in western Transbaikalia [7] and albitites of the Alakha stock in the Altai [20, 21]. The similarity of REE patterns in the most differentiated Raumid granites of phase 8 and the amazonite granites of Bezymyanka suggests a similar mechanism of their formation. In contrast, the REE patterns of the severely metasomatized Alakha albitite (normative albite is higher than 90% in some of these rocks [20]) strongly differ from those of rare-metal granites. The geochemical signatures of rare-metal granites could not be evidently produced by postmagmatic alteration only. In particular, the absence of a Eu anomaly in these rocks was explained by Abramov [22], who thermodynamically modeled REE migration in a fluoride hydrothermal solution [22]. It was shown that under these conditions, Eu exhibits no anomalous properties compared with other trace elements, because this fluid provides its highest oxidation state, Eu^{+3}. This is probably why Eu anomalies are weakly pronounced or completely absent in the albitites of the Alakha stock (Fig. 8).

Of special interest is the distinct positive correlation between Sm/Nd and Rb/Sr ratios in the granites of the Raumid Pluton (Fig. 9). Similar relations were observed in the majority of highly evolved silicic rocks of the world, including rare-metal granites [17]. These relationships are in conflict with the observed negative correlation between Nd and Sr isotopic ratios in both crustal and mantle rocks [17]. The well-known negative correlation between Sr and Nd isotope compositions in various rocks suggests a similar negative correlation between the Sm/Nd and Rb/Sr ratios in their sources. This definitely indicates that granitoids similar to the Raumid granites do not significantly contribute to the protoliths of other rocks. This is probably related to their low abundance in the Earth's crust or to the fact that highly evolved hypabyssal granites are not involved into remelting processes.

CONCLUSIONS

Wide compositional variations in the granites of the Raumid Pluton are consistent with petrographic and field observations and indicate that fractional crystallization was the leading process of their differentiation. Consistent trends in binary trace-element diagrams and systematic changes in normalized REE distribution patterns confirm a genetic relation between the granites of all intrusive phases. Superimposed greisenization disturbed the magmatic trace-element trends.

Variations in trace element (Rb, Sr, Ta, Nb, and others) contents and ratios (Rb/Sr, Ka/Lu, Eu/Eu*, and others) in the Raumid granite overlap almost the entire range of various granites, from the least differentiated rocks with ordinary contents of trace elements to rare-metal granites. This fact unambiguously indicates that the geochemical signature of rare-metal granites could be formed during the magmatic stage by the fractional crystallization of melts, which can be exemplified by the formation of the Raumid granite.

ACKNOWLEDGMENTS

This study was supported by the Russian Foundation for Basic Research, project nos. 05-05-64699 and 06-05-65239.

REFERENCES

1. A. A. Beus, V. A. Severov, A. A. Sitnin, and K. D. Subbotin, *Albitized and Greisenized Granites (Apogranites)* (Akad. Nauk SSSR, Moscow, 1962) [in Russian].
2. D. V. Rundkvist, "Modern Concepts on the Geological Structure and Zoning of the Cornwall Deposits (England)," Geol. Rudn. Mestorozhd. **22** (6), 3–17 (1980).
3. L. F. Syritso, *Mesozoic Granitoids of Eastern Transbaikalia and Problems of Rare-Metal Mineral Resources* (St. Petersb. Gos. Univ., St. Petersburg, 2002) [in Russian].
4. R. E. Van Alstine, "Continental Rifts and Lineaments Associated with Major Fluorspar Districts," Econ. Geol. **71**, 977–987 (1976).
5. F. A. Letnikov, "Magma-Forming Fluid Systems of the Continental Lithosphere," Geol. Geofiz. **44**, 1262–1269 (2003).
6. V. I. Kovalenko, *Petrology and Geochemistry of Rare-Metal Granites* (Nauka, Novosibirsk, 1977) [in Russian].
7. V. I. Kovalenko, Yu. A. Kostitsyn, V. V. Yarmolyuk, et al., "Magma Sources and the Isotopic (Sr and Nd) Evolution of Li–F Rare-Metal Granites," Petrologiya **7**, 383–409 (1999) [Petrology **7**, 383–409 (1999)].
8. V. N. Volkov and E. V. Negrei, "Structure of the Raumid Pluton and the Problem of Emplacement of Granite Intrusions," Sov. Geol., No. 3, 46–59 (1974).
9. V. N. Volkov, "Genesis of the Vertical Zoning of the Raumid Granite Pluton (Southern Pamirs)," Izv. Akad. Nauk SSSR, Ser. Geol., No. 6, 52–63 (1990).
10. Yu. A. Kostitsyn and V. N. Volkov, "Heterogeneity of the Primary Strontium Isotope Composition and Petrogenesis of the Raumid Pluton (Southern Pamirs)," Geokhimiya, No. 6, 853–864 (1989).
11. V. N. Volkov and S. A. Gorbacheva, "Changes in the Crystallization Conditions of Granites in a Vertically Exposed Intrusion: Data on Biotite Composition," Geokhimiya, No. 1, 147–153 (1980).
12. V. N. Volkov, R. D. Gavrilin, and Z. A. Kotel'nikova, "Distribution of K, Na, Li, and Rb in the Vertical Sections and Age Series of a Multiple Granite Massif," Geokhimiya, No. 9, 1379–1394 (1978).
13. N. M. Evensen, P. J. Hamilton, and R. K. O'Nions, "Rare-Earth Abundances in Chondritic Meteorites," Geochim. Cosmochim. Acta **42**, 1199–1212 (1978).
14. L. A. Haskin, "Petrogenetic Modelling—Use of Rare Earth Elements," in *Rare Earth Element Geochemistry*,. Ed. by P. Henderson (Elsevier, Amsterdam, 1984), pp. 115–152.
15. P. Henderson, *Inorganic Geochemistry* (Pergamon, Oxford, 1982).
16. H. Nagasawa, "Partitioning of Eu and Sr between Coexisting Plagioclase and K-Feldspar," Earth Planet. Sci. Lett., **13**, 139–144 (1971).
17. Yu. A. Kostitsyn, "Source of Rare Metals in Peraluminous Granites: A Review of Geochemical and Isotopic Data," Geochem. Int. **39**, Suppl. 1, 43–59 (2001).
18. L. P. Gromet and L. T. Silver, "Rare Earth Element Distributions among Minerals in a Granodiorite and Their Petrogenetic Implications," Geochim. Cosmichim. Acta **47**, 925–939 (1983).
19. D. W. Mittlefehldt and C. F. Miller, "Geochemistry of the Sweetwater Wash Pluton, California: Implications for 'Anomalous' Trace Element Behavior during Differentiation of Felsic Magma," Geochim. Cosmochim. Acta **47**, 109–124 (1983).
20. A. G. Vladimirov, S. P. Shokal'skii, A. P. Ponomareva, et al., "Late Paleozoic–Early Mesozoic Granitoid Magmatism of the Altai," Geol. Geofiz., No. 4, 3–17 (1997).
21. Yu. A. Kostitsyn, S. A. Vystavnoi, and A. G. Vladimirov, "Age and Genesis of the Spodumene-Bearing Granites of the SW Altai (Russia): An Isotopic and Geochemical Study," Acta Univ. Carolinae Geol. **42**, 60–63 (1998).
22. S. S. Abramov, "Modeling of REE Fractionation in the Acid Melt–Fluoride–Chloride Fluid System," Dokl. Akad. Nauk **376**, 1–3 (2001) [Dokl. Earth Sci. **377**, 198–200 (2001)].